Referência Completa da Publicação:

MAGRINI, L. A.; DOMINGUES, M. O; MACAU, E. E. N.; KISS, I. Z. Extraction of slow and fast dynamics of multiple time-scale systems using wavelet techniques.**Chaos: An Interdisciplinary Journal of Nonlinear Science**, v. 30, n. 6, 2020.

Extraction of Slow and Fast Dynamics of Multiple Time-Scale Systems Using Wavelet Techniques

Luciano Aparecido Magrini,[1,2,a] Margarete Oliveira Domingues,[3,4,b] Elbert E. N. Macau,[5,6,c] and István Z. Kiss[7,d]

[1] *Federal Institute of Education, Science and Technology of São Paulo (IFSP), São Paulo, ZIP CODE 01109-010, Brazil.*

[2] *Graduation Program of Applied Computing (CAP/INPE), São José dos Campos, ZIP CODE 12227-010, Brazil.*

[3] *National Institute for Space Research (INPE), São José dos Campos, ZIP CODE 12227-010, Brazil.*

[4] *Associated Laboratory of Computation and Applied Mathematics (LabAC), São José dos Campos, ZIP CODE 12227-010, Brazil.*

[5] *Associated Laboratory of Computation and Applied Mathematics (LabAC)*

[6] *Federal University of São Paulo at São José dos Campos (UNIFESP), São José dos Campos, ZIP CODE 12231-280, Brazil.*

[7] *Department of Chemistry, Saint Louis University, 3501 Laclede Ave, St Louis, MO 63103, USA.*

(Dated: 14 December 2020)

A methodology is presented based on wavelet techniques to approximate fast and slow dynamics present in time-series whose behavior is characterized by different local scales in time. These approximations are a useful to understand the global dynamics of the original, full systems, especially in experimental situations, where all information is contained in a one-dimensional time-series. Wavelet analysis is a natural approach to handle these approximations because each dynamical behavior manifests its specific subset in frequency domain; for example, with two time scales the slow and fast dynamics are present in low and high frequencies, respectively. The proposed procedure is illustrated by the analysis of a complex experimental time-series of iron electrodissolution, where the slow, chaotic dynamics is interrupted by fast irregular spiking. The method can be used to first filter the time-series data, and then separate the fast and slow dynamics even when clear maxima and/or minima in the corresponding global wavelet spectrum are missing. The results could find applications in the analysis of synchronization of complex systems through multi-scale analysis.

Complex behavior in natural systems are often generated by interactions of periodic phenomena with largely different time-scales. For example, heart rate variations can be affected by neuronal firings, breathing, or sleep-wake patterns. When the time-scales of such processes are well separated and the behavior is highly periodic, the signals can be analyzed with simple low and high-pass filters. In this work, we consider a very complex electrochemical behavior, the corrosion of iron in an acid. A wavelet-based methodology is presented, where the slow and fast time scales can be separated even with chaotic slow and irregular fast spiking.

I. INTRODUCTION

Systems with different processes taking place over separate time scales are ubiquitous in a large range of phenomena in areas such as physics (e.g. lasers[1,2], forced Van der Pol oscillators[3], Faraday waves[4]), chemistry (e.g.,homogeneous reactions[5] and electrochemical phenomena[6]), biology (e.g., neural activity[7,8], cardiac[9] and β-pancreatic[10] cells) and other[11–13]. In the most common scenario there are fast and slow dynamics, where the slow variable acts as a slowly varying 'parameter' in the fast subsystem. With oscillatory dynamics, the time series consist of fast, repetitive bursting interrupted by slow, acquiescent, dynamics where the oscillations are smooth and the wavelength is large in comparison with the bursting. System description and technological applications require the separation of the system time scales. This is the case, for example in neuronal and climate systems and the corresponding control applications. In particular, this separation is of importance to characterize synchronization phenomena in nonlinear systems[14–18]. Several studies have investigated approaches to separate the fast and slow dynamics[19–21]. For example, one can take advantage of the known eigenvalues and eigenvectors of the full system[19] or apply computational methods based on identification of low dimensional surface trajectories in phase space[20]. Separation can help construction of slow invariant manifolds with fast relaxations[21] to overcome the numerical difficulties of integration of stiff systems[22]. Therefore, with experimental data, it is essential to properly extract the fast and slow dynamics so that accurate models can be formulated. When the underlying dynamics are relatively simple (e.g., simple periodic oscillations with a well-defined frequency), combination of low-pass, high-pass, and band-pass FFT filters can be used to process data[23]. However, when the underlying dynamics are more complex (e.g., chaotic or oscillations with largely varying frequencies and

[a] magrini@ifsp.edu.br
[b] margarete.domingues@inpe.br
[c] elbert.macau@unifesp.br
[d] izkiss@slu.edu

amplitudes), automatic processing of large amount of data can be challenging. In this paper, a wavelet-based technique is presented that allows the proper separation of slow and fast dynamics from experimental data, as well as de-noise the signal at the same time. The method was developed aiming the analysis of an electrochemical process, the iron dissolution in sulfuric acid, which exhibits fast periodic spiking in a large frequency range with a highly complex, chaotic slow dynamics. The data was collected from a coupled pair of oscillators with different coupling strengths. The occurrence of the irregular bursting activities, affected by the coupling, along the chaotic trajectories demanded a versatile technique to separate noise, and fast and slow oscillations. The method is based on wavelet transform, exploiting its remarkable characteristic that allows time-scale analysis for performing the identification of different behaviors in time-domain[24] associating then with different frequency sub-bands. The article is organized as follows. Section II presents the proposed approach to separate fast and slow dynamics. The data collection details are described in Sections V and III. Section IV illustrates the application in details and discusses the results. Finally, the conclusions are in Section V.

II. METHODOLOGY

This section describes the proposed methodology to unveil fast and slow dynamics embedded in a time series. Our approach is based on a continuous wavelet transform (CWT) that is used to reliably identify dynamics in the frequency of the time-series $I(t)$. In the first step, noise is removed from the time series using non-linear filtering[25]. In the sequence the wavelet analysis is performed applying the continuous wavelet transform (CWT) with L_1 norm in the frequency domain according to[26]:

$$W_I^{\psi}(a,\tau) = \frac{1}{a}\int_{-\infty}^{\infty} \mathcal{F}(I;\omega)\mathcal{F}^*(\psi;\omega,a,\tau)(\mathrm{e}^{i\omega\tau})\,d\omega, \quad (1)$$

where τ is a translation parameter in time domain, $\mathcal{F}(I;\omega)$ denotes the Fourier transform of the signal $I(t)$, $\mathcal{F}^*(\psi;\omega,a,\tau)(a\omega)$ is the conjugate of wavelet function $\psi(t)$, defined in frequency domain and calculated at $a\omega$ for each real positive value, a, called scale and related to the central pseudo-frequency[27] given by $\omega = \dfrac{\omega_c}{a\Delta t}$, where Δt is the sampling time for the measurement signal $I(t)$, and ω_c the central frequency of wavelet $\psi(\omega)$. The wavelet function considered here is the Morse wavelet, defined in the frequency domain[28–31] by:

$$\psi(\beta,\gamma,\omega) = 2(\mathrm{e}\gamma\beta)^{(\beta/\gamma)}\; U(\omega)\; \omega^{\beta}\; \mathrm{e}^{(-\omega^{\gamma})}, \quad (2)$$

where γ and β are real positives dimensionless parameters that control the waveform, regulating the frequency-domain and time-domain decay, respectively[31], $U(\omega)$ is the Heaviside step function. Morse wavelet function is analytic, therefore in a time-frequency analysis of any real signal all non-positive frequencies are zero. This property is important because it avoids the detection of small spurious negative frequencies that could influence our results. It is important to highlight that the real parameters γ and β in Equation (2) are similar to the parameters scale a and translation τ used in the usual definition of the CWT given by Equation (1). The chosen parameters are $\gamma = 3$ and $\beta = 20$. The value $\gamma = 3$ is suggested in the literature as standard value for analysis of oscillatory signals, as it is highly related with Gaussian with zero skewness[29–31]. The parameter $\beta = 20$ controls the wavelet length in time-domain. Consequently, usually large values are considered. This choice implies that the wavelet function is highly oscillatory in time-domain and therefore the resolution in frequency domain is increased[31]. More details about the choice of parameters γ and β can be found in references[29–31]. Figure (1) shows Morse wavelet in time- and frequency-domain. Notice that the behavior in frequency-domain is related with the Gaussian distribution and, in time-domain exhibits an oscillatory behavior. The magnitude scalogram defined by absolute

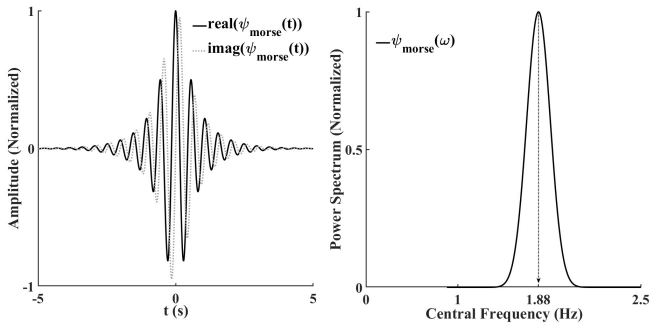

FIG. 1. Morse wavelet with $\beta = 20$ and $\gamma = 3$ in time-domain (left) and, in frequency-domain (right).

value of measures $W_I^{\psi}(a,\tau)$ allow us to calculate the global wavelet spectrum $G(\omega)$:

$$G(\omega) = \int_{-\infty}^{\infty} |W_I^{\psi}(\omega,\tau)|^2\, d\tau. \quad (3)$$

As it was previously noted[24] the high frequency bursts could not be easily extracted using the Fourier spectrum, but the global wavelet spectrum provides a better approach. (Indeed, roughly speaking, the global wavelet spectrum can be seen as a smooth version of the Fourier spectrum[32–34]). The central idea in our approach is that by a careful analysis of $G(\omega)$ it is feasible to localize sub-bands Ω_{slow} and Ω_{fast}, whose content corresponds to each time scale. These sub-bands of the wavelet transform are used to reconstruct time domain signals associated with the underlying time scales using the inverse continuous wavelet transform (ICWT). For this purpose, it is necessary to know the upper and lower extremes of the intervals Ω_{slow} and Ω_{fast} (Hz). Ideally, the fast and the slow oscillations generate a global wavelet spectrum with two dominant frequency peaks. Let $\omega_{\max}^{slow}$ and $\omega_{\max}^{fast}$ be the frequencies where global wavelet spectrum $G(\omega)$ exhibits the largest peaks related with the slow and the high frequency content. If the amplitude of the these two peaks are sufficiently large, then there will be a local minimum at a fre-

quency $m_{slow} \geq \omega_{\max}^{slow}$. Similarly, at the peak corresponding to the fast time scale, there will be a minimum just below the dominant peak $m_{fast} \leq \omega_{\max}^{fast}$. The slow dynamics thus can be represented by the frequency components from zero up to m_{slow}: $\Omega_{slow} =]0, m_{slow}]$. The fast dynamics contains frequencies from m_{fast} to the maximum frequency $\omega_{\max}$: $\Omega_{fast} = [m_{fast}, \omega_{\max}]$. See general scheme in Figure 2. After a careful analysis of a large body of collected experimental data, we found that in some examples m_{slow}, m_{fast} and/or the peaks $\omega_{\max}^{slow}$ and $\omega_{\max}^{fast}$ cannot be well-defined in the global wavelet spectrum. In these cases, two alternative strategies can be followed. If the value m_{slow} cannot be determined by analysis of global wavelet spectrum $G(\omega)$ then $2\omega_{\max}^{slow}$ was chosen as upper extreme for interval Ω_{slow}. The choice for $2\omega_{\max}^{slow}$ was done empirically: we analyzed each case and possible choices for ω_{slow}; the value $2\omega_{\max}^{slow}$ presented better results for the slow dynamics approximation process. In this case, the lower extreme is equal to smallest frequency ω_{slow} detected in time-frequency analysis.

If it is not possible to localize well-defined peak $\omega_{\max}^{fast}$ in $G(\omega)$ then the lower extreme for Ω_{fast} must be chosen at an inflection point in $G(\omega)$. In this case, the upper extreme is equal to largest frequency ω_{fast} detected in time-frequency analysis. After determining Ω_{slow} and Ω_{fast}, the approximations $I_{slow}(t)$ and $I_{fast}(t)$ to slow and fast dynamics present in the signal $I(t)$ are obtained using the ICWT considering the frequency bands Ω_{slow} and Ω_{fast}, respectively. Then, we considered the computation in each case as a possible approximation for each different dynamics. We note that for identification of repetitive fast spiking events, one has to set a threshold amplitude at which the event is relevant (limiarization). Such additional step is unavoidable to discard isolated spike or other behaviors close to discontinuities in the time domain.

III. DATA COLLECTION AND EXPERIMENTAL SETUP

The experimental time series was collected during iron electrodissolution in 1 mol/L sulfuric acid. The experiments were performed in an electrochemical cell consisting of 0.5 mm diameter iron working, Hg/Hg_2SO_4 / sat. K_2SO_4 reference, and Pt counter electrodes. When the potentiostat applies constant circuit potential V with respect to the reference electrode, the current $I(t)$ can be measured with zero resistance ammeter at a sampling rate of 1000 Hz. In a previous study[6], it was shown that bursting current oscillations can occur when 1 kOhm external resistance is attached to the iron wire. The time-series data exhibited slow chaotic variations, which were interrupted with high-frequency bursting. Here we consider an even more complex system, where two iron wires dissolve simultaneously. The electrodes were connected to the potentiostat through two individual parallel resistors (R_{ind}) and one series collective resistor (R_{coll}), in such a way that the total resistance $R_{\text{tot}} = R_{\text{ind}} + 2R_{\text{coll}}$ was kept constant, but the collective resistance fraction $\varepsilon = 2R_{\text{coll}}/R_{\text{tot}}$ was changed. The collective resistance introduces electrical coupling between the wires, whose strength can be controlled with ε. Such coupling can greatly enhance the complexity of the individual time series of the chaotic system. As shown in Table I such experiments were performed, and two time series were collected for wires 1 and 2, respectively. The coupling strength ε was varied between 0 (no coupling) and 1 (strong coupling).

IV. RESULTS AND DISCUSSIONS

This Section presents the results obtained with the application of the proposed methodology in the computation of approximations for fast and slow dynamics of the experimental data set described in Section III.

A. Scalograms with two well-defined peaks

The top panel in Figure 3 shows the typical behavior of time-series with chaotic slow dynamics and irregular burstings over the fast dynamics (only the initial ten seconds are shown for better visualization). Visual inspection of the scalogram (bottom panel in Figure 3) reveals that the fast subsystem (the bursting intervals) corresponds to frequencies larger than approximately 30 Hz and the slow subsystem corresponds to the frequencies between 3 Hz and 10 Hz, approximately. These frequency ranges can be better inferred from the the global wavelet spectrum (right plot in bottom panel); the spectrum exhibits two different and well-defined peaks: One around 4 Hz and other around 60 Hz (the exact values are 3.91 Hz and 58.37 Hz, respectively). Note that the system exhibits complex dynamics, whose behavior cannot be localized to narrow frequency bands. Instead, some contribution to the slow and the fast subsystems occur with frequencies above and below 100 Hz and 3 Hz, respectively. In Figure 4 the scalograms are shown for the first 10 s of the time-series listed in Table I: While the complexity of the time series is certainly different, the fast and slow dynamics manifest, approximately, in the same frequency ranges. The separation of the fast and slow dynamics using the wavelet transform, in the most trivial case is explained with dataset A (see Figure 3 for the time series). In this example, there are well-defined *minima* below the fast ($m_{fast} = 34.7$ Hz) and above the slow (m_{slow} = 7.2 Hz) peaks in the global wavelet spectrum $G(\omega)$ as can be seen in Figure 5. Therefore, the fast and slow dynamics corresponds to frequency sets $\Omega_{fast} = [34.7, 434.1]$ Hz and $\Omega_{slow} =]0, 7.2]$ Hz. In order to generate the approximations to dynamics, namely $I_{fast}(t)$ and $I_{slow}(t)$, the ICWT was performed using the sets $\Omega_{fast} = [34.7, 434.1]$ Hz and $\Omega_{slow} =]0, 7.2]$ Hz and considering zero all others frequency contents. The results can be seen in Figure 6. The slow approximation $I_{slow}(t)$ captures very well the behavior of largest amplitude, slow oscillations in time-domain; for example, comparison of panels A and C in Figure 6 reveals that the number of oscillations and their shapes are preserved. The analysis for fast dynamics is more subtle: notice that the repetitive fast oscillations are correctly localized in B, although there are small amplitude burstings that are not easy to recognize in the original current $I(t)$. These spuri-

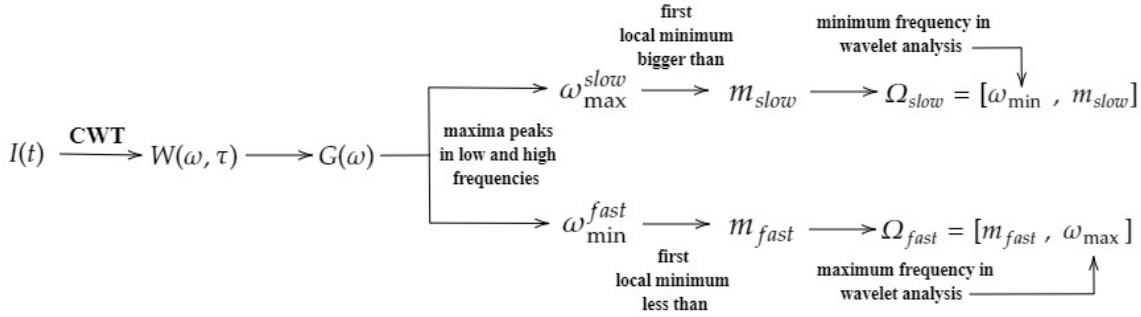

FIG. 2. General scheme to found sets Ω_{slow} and Ω_{fast} in typical case.

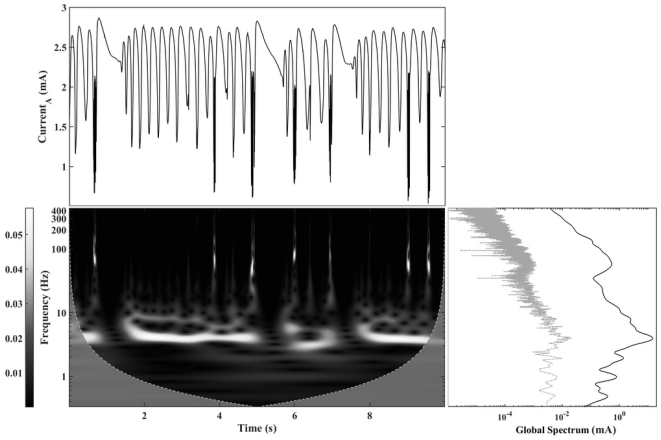

FIG. 3. Typical behavior in time-domain to current in data A with $\varepsilon = 0.0$ and respective scalogram with Fourier (gray) and global wavelet spectrum (black). Shifted for better visualization.

ous small burstings correspond to regions in the original data whose time behavior is very similar to a single isolated spike. As such, we do not consider them as bursting regions. A possible way to eliminate such regions is to limiarize $I_{fast}(t)$: The CWT of $I_{fast}(t)$ is performed, the scalogram is integrated over frequency. The Figure 7 shows that this procedure is able to detect the seven bursting regions in the given time series. The time series of two of these bursts are shown Figure 8. The original (top) and the reconstructed (bottom) burstings are similar in the sense that they have the same number of cycles and the cycles have similar waveforms.

B. Scalograms without two well-defined peaks

While one could expect that the above described procedure can be routinely applied to data sets with fast and slow dynamics, the difficulties of separating the two time scales are illustrated using data C in Table I; the global wavelet spectrum is shown in Figure 9. In this case, the maximum of the slow peak is well-defined with $\omega_{\max}^{slow} = 5$ Hz. However, there is no clear minimum above the slow peak that could define m_{slow}. In such examples, we found that very good reconstruction of the slow dynamics can be achieved by setting $m_{slow} = 2\omega_{\max}^{slow}$, i.e., in this example $m_{slow} = 10$ Hz. The analysis of the high-frequency region is even more complicated, because there is no clear maximum. However, notice that there is an inflection point in the global wavelet spectrum at around $F = [70, 110]$ Hz. In such examples, we found that the fast dynamics can be reconstructed assuming that $m_{fast} = 90$ Hz (basically, we used the mean between the 110Hz and 90Hz), and thus the reconstruction is made with all the frequencies above this threshold. Using subsets $\Omega_{slow} =]0, 10]$ Hz and $\Omega_{fast} = [90, 434.1]$ Hz the approximations were calculated (see Figure 10); with these ranges the largest oscillations were preserved in slow approximation and the burstings were correctly identified in fast approximation. Figure 11 shows that the waveform and number of spikes in burstings in fast approximation are the same that in the experimental current.

C. Pitfalls of finding frequency intervals

Finally, we must emphasize, that the broad-range frequencies are essential to properly characterize the complex dynamics of the system. In other words, a simple pass-through filter can dramatically change the waveform of oscillations, which can misrepresent the corresponding dynamics. For example, the waveform deformation is illustrated with dataset A in Figure 12. If the range range $[2.4, 7.2]$ Hz is used instead of the proposed $]0, 7.2]$ Hz, the slow dynamics can exhibit spurious oscillations close to bursting dynamics or during a quite acquiescence period (e.g., see time domains I, II, and III). In relation to fast approximation, similar effect can be observed if high-frequency components are discarded. Figure 13 shows two bursting regions in dataset E, where the proposed $[47, 434.1]$ Hz range is replaced with a narrower, $[47, 88]$ Hz range around the maximum. Notice that the bursting regions in the narrow band approximation (panel C) do not preserve waveform and number of spikes, that is, the approximation to fast dynamics is not correct. Table I summarizes which approximations were applied to reconstruct the slow and fast dynamics from the experimental data. (The time and frequency values are rounded to the nearest integer.) Out of the sixteen data sets, only three exhibited well defined maximum and surrounding minima in the global wavelet spectrum that could be used for the approximations (datasets A, H, M). In one

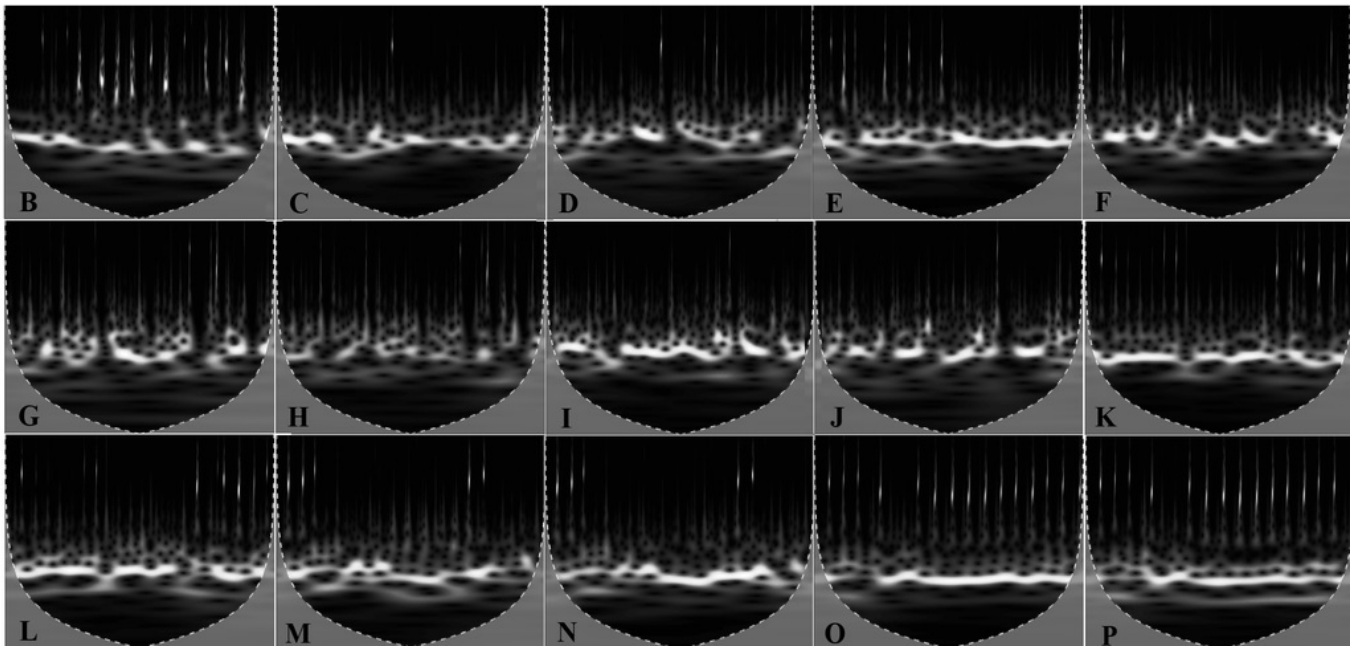

FIG. 4. Scalograms to time-series described in Table I. The frequency band, time and colorbar ranges are the same of Figure 3.

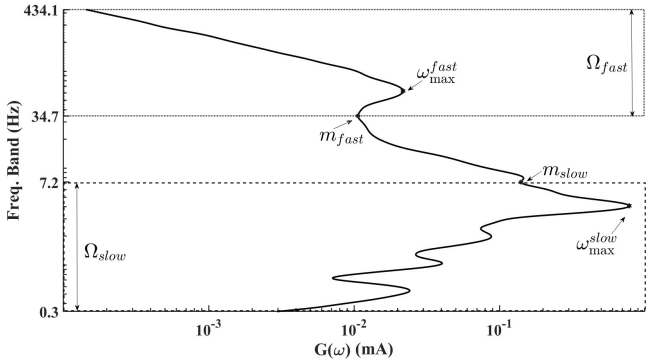

FIG. 5. Sets Ω_{fast} and Ω_{slow} to fast and slow approximations to data A whose $\varepsilon = 0.0$: frequency range $]7.2, 34.7[$ Hz is not used to build approximations.

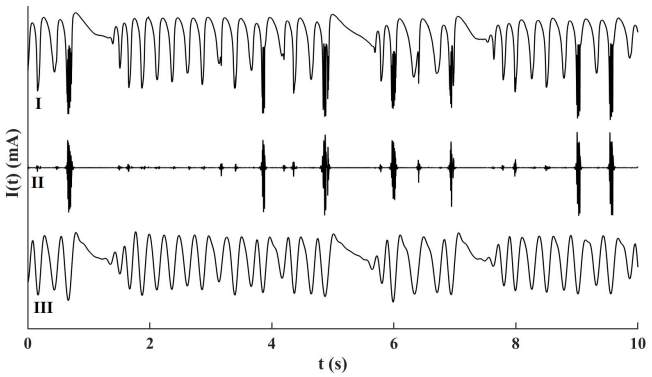

FIG. 6. The experimental current (I) and approximations to fast and slow dynamics (II and III) reconstructed using $\Omega_{fast} = [34.7, 434.1]$ Hz and $\Omega_{slow} =]0, 7.2]$ Hz. For better visualization only initial ten seconds are plotted and the approximation time-series are shifted. Representation using data A with $\varepsilon = 0.0$.

example, (dataset B), only m_{fast} was missing. In a typical data set (11 examples), m_{slow} was not used, and thus we used $m_{slow} = 2\omega_{\max}^{slow}$. With the the most difficult dataset C, only $\omega_{\max}^{slow}$ could be identified. Nonetheless, as described above, with the proposed methodology presented, we succeeded in reconstructing the fast and slow dynamics with an automated range identification based on the global wavelet spectrum.

V. CONCLUSION

The proposed analysis was found to be useful in locating frequency intervals, by which the slow and fast dynamics of the complex multi-scale system can be separated. The method can be used to first filter the time-series data, and then separate the fast and slow dynamics even when clear maxima and/or minima in the corresponding global wavelet spectrum are missing. The method was applied to the chaotic iron electrodissolution system, where the chaotic, slow dynamics made the identification of the fast bursting regions challenging. It was demonstrated that with such broad-frequency dynamics, application of simple pass-through filters are problematic. The methodology could facilitate analysis of synchronization of bursting oscillations, where separate analysis could be performed for the synchronization of the slow and the fast oscillations.

Time-Series	Length (seconds)	Coupling Strength (ε)	Peaks		Local Minima		Approximation Sets	
			$\omega_{\max}^{slow}$	$\omega_{\max}^{fast}$	m_{slow}	m_{fast}	Ω_{slow} **(Hz)**	Ω_{fast} **(Hz)**
A	60	0.0	4	62	7	33	]0, 7]	[33, 434]
B	60	0.0	4	36	14	*	]0, 14]	[36, 434]
C	235	0.2	5	*	*	*	]0, 10]	[90, 434]
D	235	0.2	4	88	*	50	]0, 8]	[50, 434]
E	150	0.4	4	66	*	47	]0, 8]	[47, 434]
F	150	0.4	5	76	*	66	]0, 10]	[66, 434]
G	55	0.6	5	176	*	143	]0, 10]	[143, 434]
H	55	0.6	4	134	5	101	]0, 5]	[82, 434]
I	82	0.7	5	94	*	82	]0, 5]	[82, 434]
J	82	0.7	5	101	*	82	]0, 5]	[82, 434]
K	120	0.8	5	94	*	82	]0, 5]	[82, 434]
L	120	0.8	5	101	*	82	]0.5]	[82, 434]
M	100	0.9	4	88	8	44	]0, 8]	[44, 434]
N	100	0.9	4	88	*	41	]0, 8]	[41,434]
O	80	1.0	4	67	*	36	]0, 8]	[36, 434]
P	80	1.0	4	67	*	36	]0, 8]	[36, 434]

TABLE I. Results summary to data set analyzed. Asterisks indicates values that can not be obtained from the global wavelet spectrum. We notice that time-series with the same coupling strength are not independents.

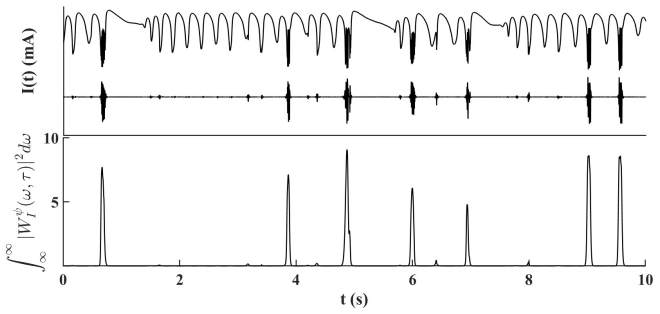

FIG. 7. The largest peaks (bottom panel) permits identify real burstings in fast approximation to original current (top panel). Representation using data A with $\varepsilon = 0.0$.

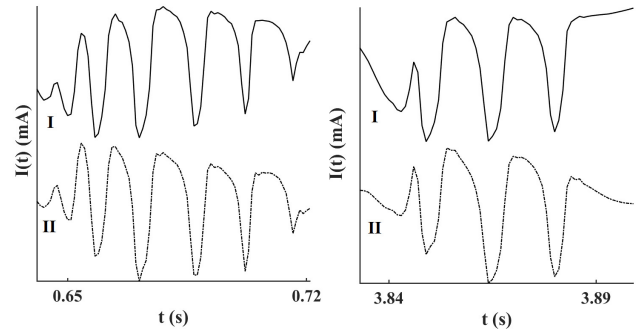

FIG. 8. Comparison between burstings in original current (I) and fast approximations (II) in time intervals $[0.64, 0.72]$ (s) and $[3.83, 3.90]$ (s) using data A with $\varepsilon = 0.0$

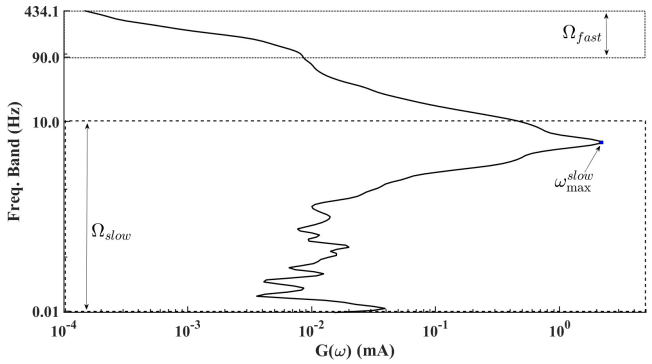

FIG. 9. Sets Ω_{fast} and Ω_{slow} to fast and slow approximations to data C with $\varepsilon = 0.2$.

ACKNOWLEDGMENTS

LM had financial support from the Coordenação de Aperfeiçoamento de Pessoal de Nível Superior - Brazil (CAPES) - Finance Code 001. MD acknowledges the financial support from Conselho Nacional de Desenvolvimento Científico e Tecnológico (CNPq), grant $302226/2018-4$. EENM is supported by grant $2015/50122-0$ of São Paulo Research Foundation (FAPESP) and grant $307714/2018-7$. IZK acknowledges support from National Science Foundation CHE-1900011 grant.

DATA AVAILABILITY

The data set that support the findings of this study are available from the corresponding author upon reasonable request with

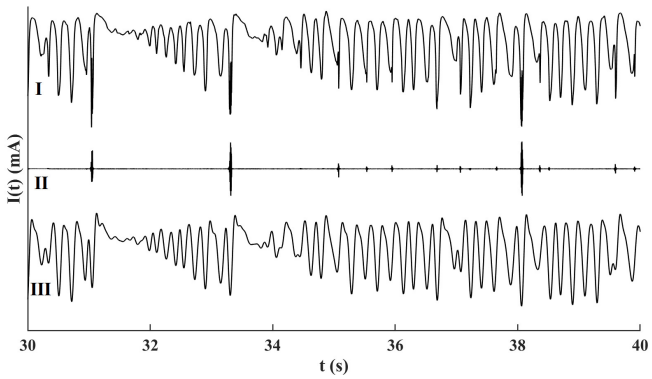

FIG. 10. The experimental current (I) and approximations to fast and slow dynamics (II and III) reconstructed using $\Omega_{fast} = [90, 434.1]$ Hz and $\Omega_{slow} =]0, 10]$ Hz (degenerate case). For better visualization only initial ten seconds are plotted and the approximation time-series are shifted. Representation using data C with $\varepsilon = 0.2$.

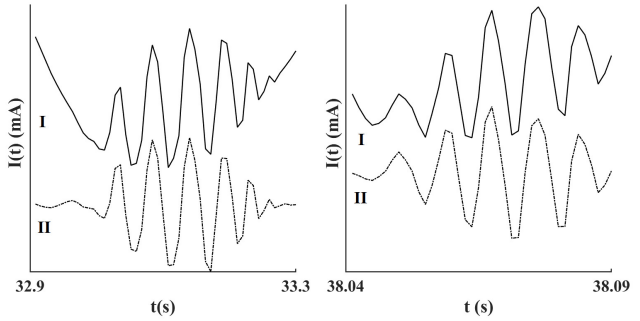

FIG. 11. Comparison between burstings in original current (I) and fast approximations (II) in time intervals $[32.9, 33.3]$ and $[38.04, 38.09]$. Representation using data C with $\varepsilon = 0.2$.

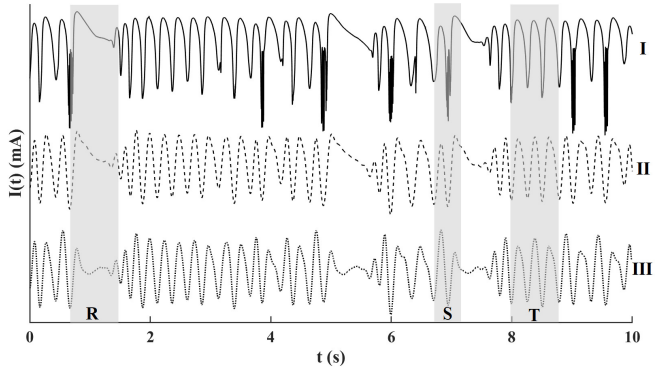

FIG. 12. Deformation regions (R, S and T) in slow approximation (III) computed with maximum peak region in low frequency ($[2.4, 7.2]$ Hz) and (II) computed with proposed methodology ($]0, 7.2]$ Hz). Compare with experimental current (I)). Representation using data C with $\varepsilon = 0.2$.

previous authorization by co-author IZK. Further details of the experiments are given in the previous publication[6].

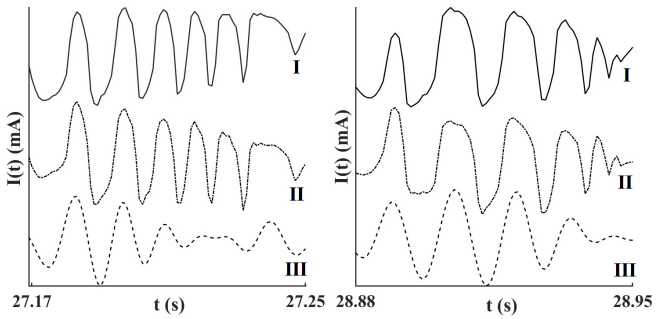

FIG. 13. Bursting regions in fast approximation (III) computed with maximum peak region in fast frequency ($[47, 88]$ Hz) and (II) computed with proposed methodology ($]47, 434.1]$ Hz). Compare with experimental current (I) to data E with $\varepsilon = 0.4$ according to Table I. The approximations are shifted to better visualization.

[1] G. Giacomelli and A. Politi, "Multiple scale analysis of delayed dynamical systems," Physica D: Nonlinear Phenomena **117**, 26–42 (1998), dOI:10.1016/S0167-2789(97)00318-7.

[2] R. Roy, T. W. Murphy, T. D. Maier, Z. Gills, and E. R. Hunt, "Dynamical control of a chaotic laser: Experimental stabilization of a globally coupled system," Physics Review Letters **68**, 1259–1262 (1992), dOI:10.1103/PhysRevLett.68.1259.

[3] M. Desroches, J. Guckenheimer, B. Krauskopf, C. Kuehn, H. M. Osinga, and M. Wechselberger, "Mixed-mode oscillations with multiple time scales," SIAM Review **54**, 211–288 (2012), dOI:10.1137/100791233.

[4] P. Chen and J. Viñals, "Amplitude equation and pattern selection in faraday waves," Phys. Rev. E **60**, 559–570 (1999), DOI:10.1103/PhysRevE.60.559.

[5] K. L. Hjertarger, B. O. Hjertarger, Perrier, and T. Solberg, "Cfd modelling of fast chemical reactions in turbulent liquid flows," Computers & Chemical Engineering **26**, 507–575 (2002), DOI:10.1016/S0098-1354(01)00799-2.

[6] I. Z. Kizz, L. Qing, O. Levent, and J. L. Hudson, "Electrochemical bursting oscillations on a high-dimensional slow subsystem," Physical Chemistry Chemical Physics **8**, 2707–2715 (2006), dOI:10.1039/B602955H.

[7] E. M. Izhikevich, "Neural excitability, spiking and bursting," International Journal of Bifurcation and Chaos **10**, 1171–1266 (2000), dOI:10.1142/S0218127400000840.

[8] E. M. Izhikevich, "Simple model of spiking neurons," IEEE Transactions on Neural Networks **14**, 1569–1572 (2003), dOI:10.1109/TNN.2003.820440.

[9] N. Naqvi, M. Li, J. W. Calvert, T. Tejada, J. P. Lambert, J. Wu, S. H. Kesteven, S. Holman, T. Matsuda, J. D. Lovelock, *et al.*, "A proliferative burst during preadolescence establishes the final cardiomyocyte number," Cell **157**, 795–807 (2014), dOI:10.1016/j.cell.2014.03.035.

[10] P. Rorsman and F. M. Ashcroft, "Pancreatic β-cell electrical activity and insulin secretion: of mice and men," Physiological Reviews **98**, 117–214 (2017), dOI:10.1152/physrev.00008.2017.

[11] X. Chen, M. Heidarinejad, J. Liu, and D. P. Christofides, "Composite fast-slow mpc design for nonlinear singularly perturbed systems," AIChE Journal **58**, 1802–1811 (2012), dOI:10.1002/aic.13798.

[12] J.-. W. Son and J.-. T. Lim, "Feedback linearisation of nonlinear singularly perturbed systems with non-separate slow-fast dynamics," IET Control Theory & Applications **2**, 728–735 (2008), dOI:10.1049/iet-cta:20070207.

[13] Y. Wang and S. Boyd, "Fast model predictive control using online optimization," IEEE Transactions on Control Systems Technology **18**, 267–278 (2010), dOI:10.1109/TCST.2009.2017934.

[14] I. Omelchenko, M. Rosenblum, and A. Pikovsky, "Synchronization of slow-fast systems," The European Physical Journal Special Topics **191**, 3–14 (2010), dOI:10.1140/epjst/e2010-01338-4.

[15] K. Fujimoto and K. Kaneko, "How fast elements can affect slow dynamics," Physica D: Nonlinear Phenomena **180**, 1–16 (2003), dOI:10.1016/S0167-2789(03)00046-0.

[16] A. Mazzino, S. Musacchio, and A. Vulpiani, "Multiple-scale analysis and renormalization for preasymptotic scalar transport," Physical Review E **71** (2005), dOI:10.1103/PhysRevE.71.011113.

[17]N. Hovakimyan, E. Lavretsky, and C. Cao, eds., *Dynamic inversion of multi-input nonaffine systems via time-scale separation*, 2006 American Control Conference (Institute of Electrical and Electronic Engineers (IEEE), Minneapolis, 2006) dOI:10.1109/ACC.2006.1657276.

[18]I. M. Held, M. Winton, K. Takahashi, T. Delworth, F. Zeng, and G. K. Vallis, "Probing the fast and slow components of global warming by returning abruptly to preindustrial forcing," Journal of Climate **23**, 2418–2427 (2010), dOI:10.1175/2009JCLI3466.1.

[19]J. Chow and P. Kokotovic, "A decomposition of near-optimum regulators for systems with slow and fast modes," IEEE Transactions on Automatic Control **21**, 701–705 (1976), dOI:10.1109/TAC.1976.1101342.

[20]A. D. Goussis and M. Valorani, "An efficient iterative algorithm for the approximation of the fast and slow dynamics of stiff systems," Journal of Computational Physics **214**, 316–346 (2006), dOI:10.1016/j.jcp.2005.09.019.

[21]E. Chiavazzo, "Approximation of slow and fast dynamics in multiscale dynamical systems by the linearized relaxation redistribution method," Journal of Computational Physics **231**, 1751–1765 (2012), dOI:10.1016/j.jcp.2011.11.007.

[22]E. Vander-Eijnden, "Fast communications: Numerical techniques for multiscale dynamical systems with stochastic effects," Communications in Mathematical Sciences **1**, 385–391 (2003).

[23]A. E. Cetin, O. N. Gerek, and Y. Yardimci, "Equiripple fir filter design by the fft algorithm," IEEE Signal Processing Magazine **14**, 60–64 (1997), DOI:10.1109/79.581378.

[24]I. Daubechies, *Ten Lectures on Wavelets* (SIAM, 1992).

[25]A. Azzalini, M. Fargie, and K. Schneider, "Nonlinear wavelet thresholding: A recursive method to determine the optimal denoising threshold," Applied and Computational Harmonic Analysis **18**, 177–185 (2005), dOI:acha.2004.10.001.

[26]J. Sadowsky, "The continuous wavelet transform: a tool for signal investigation and understanding," Johns Hopkins APL Technical Digest **15**, 306–318 (1994).

[27]P. Abry, *Ondelettes et turbulences: multirésolutions, algorithmes de décomposition, invariance d'échelle et signaux de pression* (Diderot éd., 1997).

[28]S. C. Olhede and A. T. Walden, "Generalized morse wavelets," IEEE Transactions on Signal Processing **50**, 2661–2670 (2002), dOI:10.1109/TSP.2002.804066.

[29]J. M. Lilly and S. C. Olhede, "Higher-order properties of analytic wavelets," IEEE Transactions on Signal Processing **57**, 146–160 (2009), dOI:10.1109/TSP.2008.2007607.

[30]J. M. Lilly and S. C. Olhede, "On the analytic wavelet transform," IEEE Transactions on Information Theory **56**, 4135–4156 (2010), dOI:10.1109/TIT.2010.2050935.

[31]J. M. Lilly and S. C. Olhede, "Generalized morse wavelets as a superfamily of analytic wavelets," IEEE Transactions on Signal Processing **60**, 6036–6041 (2012), dOI:10.1109/TSP.2012.2210890.

[32]J. F. Kirby, "Which wavelet best reproduces the Fourier power spectrum?" Computers & Geosciences **31**, 846–864 (2005), DOI:10.1016/j.cageo.2005.01.014.

[33]V. Perrier, T. Philipovitch, and C. Basdevant, "Wavelet spectra compared to fourier spectra," Journal of Mathematical Physics **36**, 1506–1519 (1995), DOI:10.1063/1.531340.

[34]P. Frick, D. Galyagin, D. Hoyt, E. Nesme-Ribes, K. H. Schatten, D. Sokoloff, and V. Zakharov, "Wavelet analysis of solar activity recorded by sunspot groups," Astronomy and Astrophysics **328**, 670–681 (1997).